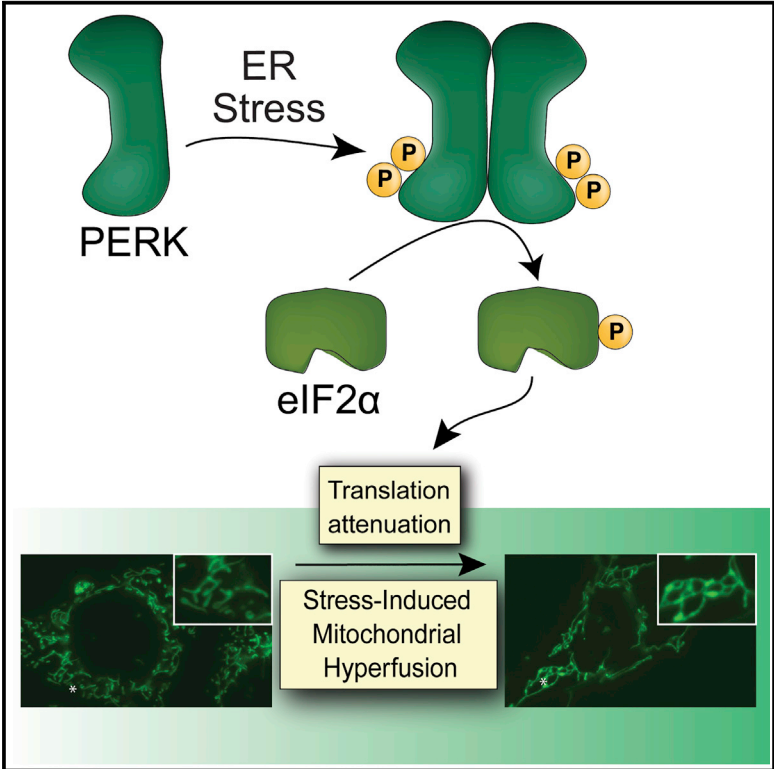


The PERK Arm of the Unfolded Protein Response Regulates Mitochondrial Morphology during Acute Endoplasmic Reticulum Stress

Graphical Abstract



Authors

Justine Lebeau, Jaclyn M. Saunders, Vivian W.R. Moraes, Aparajita Madhavan, Nicole Madrazo, Mary C. Anthony, R. Luke Wiseman

Correspondence

wiseman@scripps.edu

In Brief

Endoplasmic reticulum (ER) stress can be transmitted to mitochondria and induce pathologic mitochondrial dysfunction in association with diverse diseases. Here, Lebeau et al. show that the PERK arm of the unfolded protein response protects mitochondria during ER stress by promoting stress-induced mitochondrial hyperfusion.

Highlights

- Stress-induced mitochondrial hyperfusion (SIMH) is triggered by ER stress
- ER-stress-induced SIMH is activated by PERK-dependent translation attenuation
- PERK-regulated SIMH promotes electron transport chain activity during ER stress
- PERK integrates transcriptional and translational signaling to protect mitochondria



The PERK Arm of the Unfolded Protein Response Regulates Mitochondrial Morphology during Acute Endoplasmic Reticulum Stress

Justine Lebeau,^{1,2} Jaclyn M. Saunders,^{1,2} Vivian W.R. Moraes,^{1,2} Aparajita Madhavan,^{1,2} Nicole Madrazo,¹ Mary C. Anthony,¹ and R. Luke Wiseman^{1,3,*}

¹Department of Molecular Medicine, The Scripps Research Institute, La Jolla, CA 92037, USA

²These authors contributed equally

³Lead Contact

*Correspondence: wiseman@scripps.edu

<https://doi.org/10.1016/j.celrep.2018.02.055>

SUMMARY

Endoplasmic reticulum (ER) stress is transmitted to mitochondria and is associated with pathologic mitochondrial dysfunction in diverse diseases. The PERK arm of the unfolded protein response (UPR) protects mitochondria during ER stress through the transcriptional and translational remodeling of mitochondrial molecular quality control pathways. Here, we show that ER stress also induces dynamic remodeling of mitochondrial morphology by promoting protective stress-induced mitochondrial hyperfusion (SIMH). ER-stress-associated SIMH is regulated by the PERK arm of the UPR and activated by eIF2 α phosphorylation-dependent translation attenuation. We show that PERK-regulated SIMH is a protective mechanism to prevent pathologic mitochondrial fragmentation and promote mitochondrial metabolism in response to ER stress. These results identify PERK-dependent SIMH as a protective stress-responsive mechanism that regulates mitochondrial morphology during ER stress. Furthermore, our results show that PERK integrates transcriptional and translational signaling to coordinate mitochondrial molecular and organellar quality control in response to pathologic ER insults.

INTRODUCTION

Mitochondrial function is highly sensitive to diverse types of cellular insults, including those that induce the accumulation of misfolded proteins within the endoplasmic reticulum (ER) lumen (i.e., ER stress). ER stress influences many aspects of mitochondrial function and can promote mitochondrial-derived proapoptotic signaling through mechanisms involving mitochondrial depolarization and fragmentation (Malhotra and Kaufman, 2011; Rainbolt et al., 2014; Vannuvel et al., 2013). As such, ER stress and mitochondrial dysfunction are intricately associated in etiologically diverse diseases, including cardiovascular disorders and many neurodegenerative diseases (De Strooper and Scor-

rano, 2012; Doroudgar and Glembotski, 2013; Mercado et al., 2013; Prell et al., 2013; Verdejo et al., 2012). Considering the pathologic relationship between ER stress and mitochondria, a key question is, “What are the stress-responsive mechanisms that protect mitochondria during ER stress?”

One mechanism by which mitochondria are regulated during stress is through the adaptive remodeling of mitochondrial molecular quality control pathways involved in protein import, folding, and proteolysis (Baker et al., 2011; Quirós et al., 2015). ER stress induces remodeling of these mitochondrial quality control pathways through the PERK arm of the unfolded protein response (UPR) (Rainbolt et al., 2014). Upon activation, PERK selectively phosphorylates the α subunit of eukaryotic initiation factor 2 (eIF2 α) (Walter and Ron, 2011). This leads to transient translational attenuation and the activation of stress-responsive transcription factors such as ATF4 (Wek and Cavener, 2007). PERK-dependent ATF4 activation induces expression of mitochondrial chaperones (e.g., the mitochondrial heat shock protein 70 [HSP70] *HSPA9*) and quality control proteases (e.g., the ATP-dependent AAA protease *LON*) (Han et al., 2013; Harding et al., 2003; Hori et al., 2002). In addition, PERK-regulated translational attenuation promotes the protective degradation of the TIM17A subunit of the TIM23 import complex to attenuate mitochondrial protein import in response to stress (Rainbolt et al., 2013). This remodeling of mitochondrial molecular quality control pathways afforded by PERK-dependent translational and transcriptional signaling functions to prevent the accumulation of damaged or non-native proteins that can disrupt mitochondrial function in response to ER insults (Rainbolt et al., 2014).

Apart from stress-responsive remodeling of molecular quality control pathways, mitochondria can also be regulated through alterations in mitochondrial morphology (i.e., organellar quality control) (Chan, 2012; Shutt and McBride, 2013; Wai and Langer, 2016). Cellular insults that severely disrupt mitochondrial function can increase mitochondrial fragmentation and subsequent targeting to mitophagy (Youle and Narendra, 2011). Through this mechanism, cells remove damaged mitochondria that can perturb global cellular function and decrease survival. In contrast, other types of stress, including starvation, UV irradiation, and ribosome inhibition, induce protective mitochondrial elongation through mechanisms such as stress-induced mitochondrial hyperfusion (SIMH) (Gomes et al., 2011; Sabouny et al., 2017; Tondera et al., 2009). SIMH is a



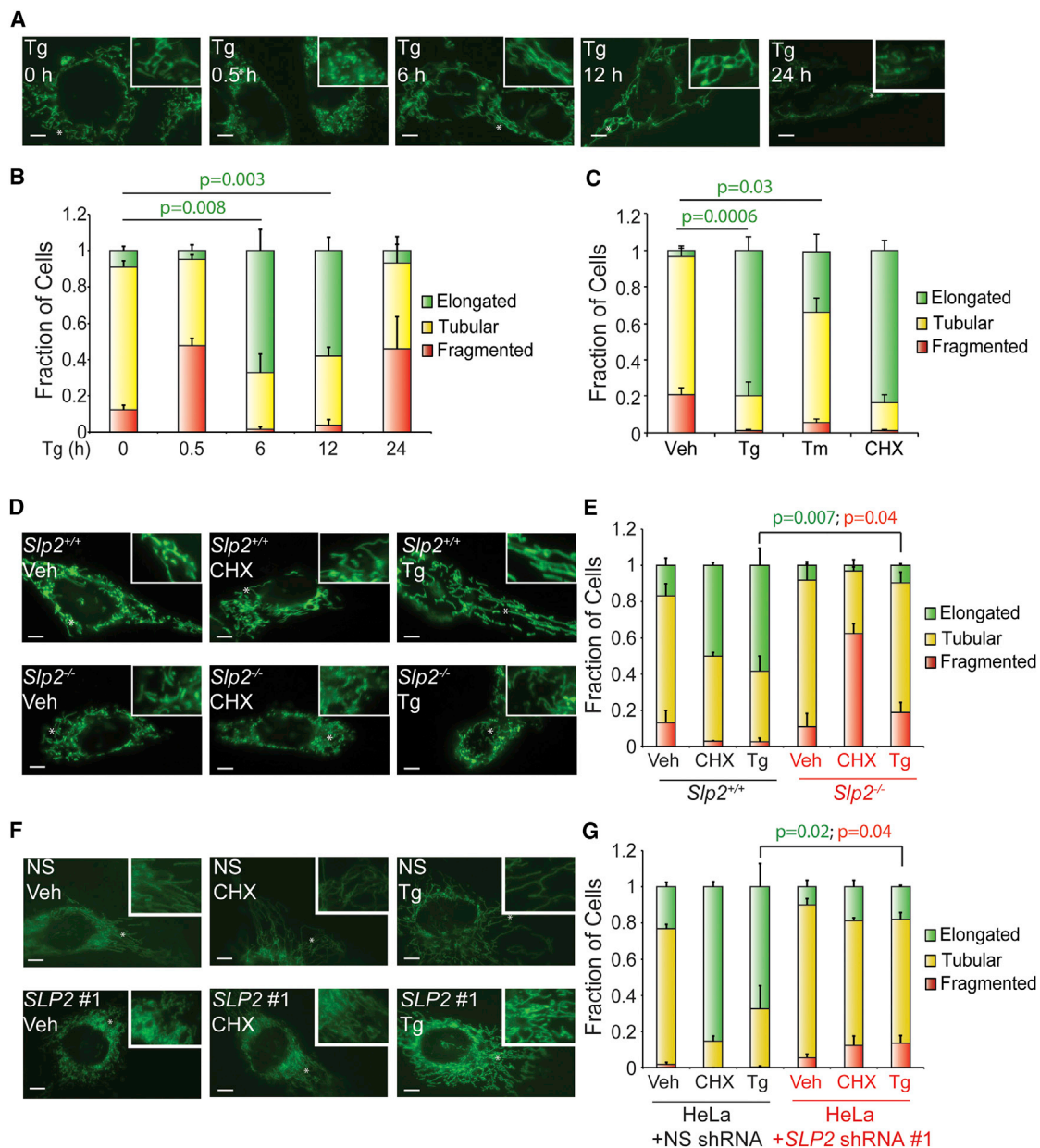


Figure 1. ER Stress Induces Stable Remodeling of Mitochondrial Morphology through SLP2-Dependent SIMH

(A) Representative images of MEF^{mtGFP} cells treated for 0, 0.5, 6, 12, or 24 hr with thapsigargin (Tg; 500 nM). The inset shows a 2-fold magnification of the image centered at the asterisk. Scale bars, 5 μ m.

(B) Quantification of fragmented (red), tubular (yellow), or elongated (green) mitochondria in MEF^{mtGFP} cells treated for 0, 0.5, 6, 12, or 24 hr with thapsigargin (Tg; 500 nM). Error bars indicate SEM from three independent experiments. p values for elongated (green text) mitochondria from a two-tailed unpaired t test are shown.

(C) Quantification of fragmented (red), tubular (yellow), or elongated (green) mitochondria in MEF^{mtGFP} cells treated for 6 hr with thapsigargin (Tg; 500 nM), tunicamycin (Tm; 1 μ M), or cycloheximide (CHX; 50 μ g/mL). Error bars indicate SEM from three independent experiments. p values for elongated (green text) mitochondria from a two-tailed unpaired t test are shown.

(D) Representative images of SLP2^{+/+} and SLP2^{-/-} MEF cells transiently transfected with mitochondrial-targeted GFP (^{mt}GFP) treated for 6 hr with cycloheximide (CHX; 50 μ g/mL) or Tg (500 nM). The inset shows a 2-fold magnification of the image centered at the asterisk. Scale bars, 5 μ m.

(E) Graph showing the fraction of SLP2^{+/+} and SLP2^{-/-} MEF cells transiently transfected with ^{mt}GFP containing fragmented (red), tubular (yellow), or elongated (green) mitochondria in cells treated for 6 hr with CHX (50 μ g/mL) or Tg (500 nM). Error bars indicate SEM for three independent experiments. p values for elongated (green text) or fragmented (red text) mitochondria from a two-tailed unpaired t test are shown.

(F) Representative images of HeLa cells stably expressing non-silencing (NS) shRNA or SLP2 shRNA #1 and transfected with ^{mt}GFP. Cells were treated for 6 hr with thapsigargin Tg (500 nM) or CHX (50 μ g/mL), as indicated. The inset shows a 2-fold magnification of the image centered at the asterisk. Scale bars, 5 μ m.

(legend continued on next page)

pro-survival mechanism that suppresses pathologic mitochondrial fragmentation and promotes mitochondrial functions such as ATP production to protect cells in response to acute insults (Chan, 2012; Shutt and McBride, 2013; Wai and Langer, 2016). Consistent with this, genetic inhibition of SIMH increases mitochondrial fragmentation, promotes mitochondrial dysfunction, and/or increases sensitivity to apoptotic stimuli (Gomes et al., 2011; Tondera et al., 2009). However, ER-stress-dependent regulation of mitochondrial morphology is currently poorly defined.

Here, we demonstrate that acute ER stress induces stable remodeling of mitochondrial morphology through SIMH. We show that ER-stress-dependent SIMH is regulated by the PERK arm of the UPR and is promoted downstream of eIF2 α phosphorylation-dependent translational attenuation. In addition, we demonstrate that pharmacologic or genetic inhibition of PERK-regulated SIMH is associated with increased mitochondrial fragmentation and impaired mitochondrial respiratory chain activity during ER stress. These results indicate that PERK-dependent SIMH is a protective mechanism to regulate mitochondrial morphology and promote mitochondrial metabolic activity in response to acute ER insults.

RESULTS

Acute ER Stress Promotes SIMH through an SLP2-Dependent Mechanism

We defined the impact of ER stress on mitochondrial morphology in wild-type mouse embryonic fibroblast (MEF^{WT}) cells stably expressing a mitochondrial-targeted GFP (MEF^{mtGFP}) following treatment with the ER stressor thapsigargin (Tg) for 0, 0.5, 6, 12, or 24 hr. We quantified mitochondrial morphology in blinded images by counting cells containing predominantly fragmented, tubular, or elongated mitochondria (see Figure S1A for examples of counting and Experimental Procedures for additional details on the quantification). Short 0.5-hr treatments with Tg increase the population of cells containing fragmented mitochondria (Figures 1A and 1B). This increase in fragmentation has previously been shown to reflect increased Ca²⁺ influx into mitochondria (Hom et al., 2007). Surprisingly, 6-hr treatments with Tg increase populations of cells containing elongated mitochondria. This increase in elongated mitochondria persisted through the 12-hr treatment, indicating that this elongation reflects a stable remodeling of mitochondrial morphology. However, prolonged 24-hr treatments with Tg induce a second round of fragmentation, which was previously associated with terminal apoptotic signaling (Hom et al., 2007). Mitochondrial elongation was also observed in MEF^{mtGFP} cells treated for 6 hr with the alternative ER stressor tunicamycin (Tm; Figures 1C and S1B) and in Tg-treated HeLa cells transiently expressing a mitochondrial-targeted GFP (mtGFP; Figures S1C and S1D). These results indicate that acute ER stress induces dynamic remodeling of mitochondrial morphology through increased elongation.

The ribosomal inhibitor cycloheximide (CHX), a compound that potently activates SIMH by promoting mitochondrial fusion (Tondera et al., 2009), increases the population of MEF^{mtGFP} cells containing elongated mitochondria to the same extent observed in Tg-treated cells (Figures 1C and S1B). CHX-dependent SIMH requires the mitochondrial scaffolding protein SLP2 (Tondera et al., 2009). If ER stress induces SIMH through a similar mechanism, we predicted that Tg-induced mitochondrial elongation would also be dependent on SLP2. We transfected SLP2^{-/-} MEFs (Mitsopoulos et al., 2015) with mtGFP and measured mitochondrial morphology following treatment with CHX or Tg. As expected, CHX-dependent SIMH is inhibited in SLP2^{-/-} MEFs (Figures 1D and 1E). Tg-dependent mitochondrial elongation is also inhibited in SLP2^{-/-} MEFs. Similar results were observed in HeLa cells expressing two different SLP2 short hairpin RNAs (shRNAs) (Figures 1F and 1G; Figures S1C–S1E). These results show that ER stress promotes SIMH through a SLP2-dependent mechanism analogous to that observed for CHX.

ER-Stress-Dependent SIMH Is Induced Downstream of PERK-Regulated Translation Attenuation

The predominant stress-responsive signaling pathway activated by ER stress is the UPR (Walter and Ron, 2011). We used a pharmacologic approach to define the contributions of the IRE1, ATF6, and PERK UPR signaling pathways on ER-stress-dependent SIMH. Pharmacologic inhibition of the IRE1 or ATF6 UPR signaling arms using 4 μ 8c (Cross et al., 2012) or Ceapin-7 (Gallagher et al., 2016; Gallagher and Walter, 2016), respectively, did not prevent Tg-induced SIMH in MEF^{mtGFP} cells (Figure S2A). However, GSK2656157 or ISRIB, two compounds that inhibit the PERK arm of the UPR through distinct mechanisms (Figure 2A) (Axten et al., 2013; Sidrauski et al., 2013), prevented Tg-induced SIMH in both MEF^{mtGFP} cells (Figures 2B–2E) and HeLa cells expressing mtGFP (Figure S2B). We confirmed that these compounds inhibit PERK-regulated transcriptional and translational signaling by qPCR and immunoblotting (Figures S2C–S2F). ISRIB similarly inhibits Tm-induced mitochondrial elongation in MEF^{mtGFP} cells (Figures 2D and 2E). However, CHX-dependent mitochondrial elongation is not affected by co-treatment with ISRIB (Figures 2D and 2E). Thus, pharmacologic inhibition of PERK-dependent eIF2 α phosphorylation using two mechanistically distinct compounds selectively disrupts ER-stress-dependent SIMH.

We further defined the involvement of PERK-dependent eIF2 α phosphorylation in ER-stress-induced mitochondrial elongation using *Perk*^{-/-} MEFs and knockin MEFs expressing the non-phosphorylatable S51A eIF2 α mutant (MEF^{A/A}) (Harding et al., 2000; Scheuner et al., 2001). Transcriptional and translational signaling induced by PERK activation is inhibited in these cells (Figure 2A). Consistent with this, both the Tg-dependent induction of *Lon*, *Hspa9*, and *Chop* and TIM17A degradation are inhibited in *Perk*^{-/-} and MEF^{A/A} cells (Figures S2G–S2I)

(G) Graph showing the fraction of HeLa cells stably expressing scrambled shRNA or SLP2 shRNA #1 and transfected with mtGFP containing fragmented (red), tubular (yellow), or elongated (green) mitochondria following treatment for 6 hr with Tg (500 nM) or CHX (50 μ g/mL), as indicated. Error bars indicate SEM for three independent experiments. p values for elongated (green text) or fragmented (red text) mitochondria from a two-tailed unpaired t test are shown.

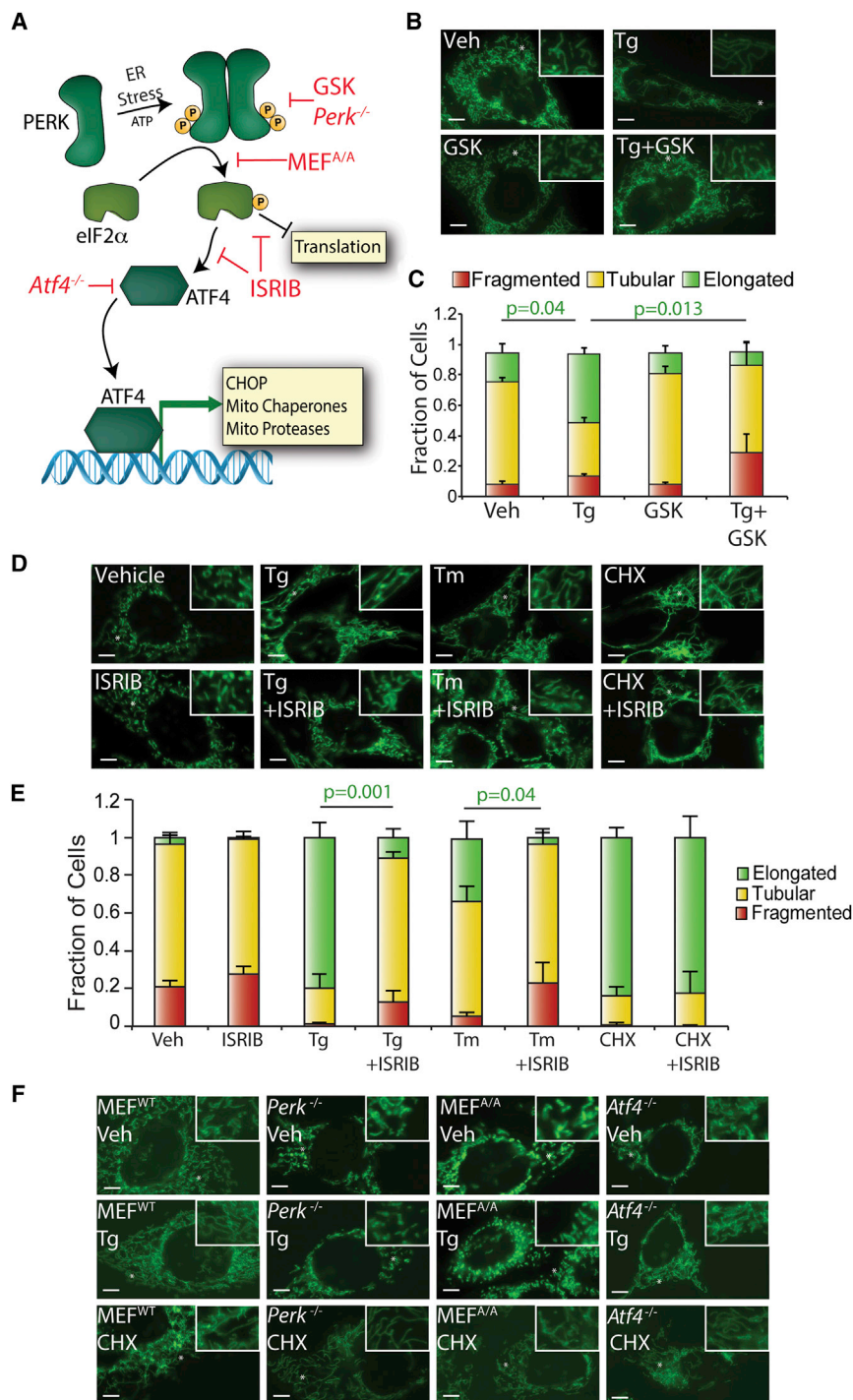


Figure 2. Pharmacologic Inhibition of the PERK UPR Signaling Arm Prevents ER-Stress-Induced SIMH

(A) Illustration showing the transcriptional and translational signaling pathways activated by PERK-regulated eIF2 α phosphorylation. Red indicates how pharmacologic and genetic disruption of PERK signaling influences PERK-regulated transcriptional and/or translational signaling.

(B) Representative images of MEF^{mtGFP} cells treated for 6 hr with thapsigargin (Tg; 500 nM) and/or the PERK inhibitor GSK2656157 (GSK; 10 μ M). The inset shows a 2-fold magnification of the image centered at the asterisk. Scale bars, 5 μ m.

(C) Quantification of fragmented (red), tubular (yellow), or elongated (green) mitochondria in MEF^{mtGFP} cells treated for 6 hr with Tg (500 nM) and/or GSK2656157 (GSK; 10 μ M). Error bars indicate SEM from three independent experiments. p values for elongated (green text) mitochondria from a two-tailed unpaired t test are shown.

(D) Representative images of MEF^{mtGFP} cells treated for 6 hr with Tg (500 nM), tunicamycin (Tm; 1 μ M), cycloheximide (CHX; 50 μ g/mL), and/or ISRIB (200 nM), as indicated. The inset shows a 2-fold magnification of the image centered at the asterisk. Scale bars, 5 μ m.

(E) Quantification of fragmented (red), tubular (yellow) or elongated (green) mitochondria in MEF^{mtGFP} cells treated for 6 hr with Tg (500 nM), Tm (1 μ M), CHX (50 μ g/mL), and/or ISRIB (200 nM). Error bars indicate SEM from three independent experiments. p values for elongated (green text) mitochondria from a two-tailed unpaired t test are shown.

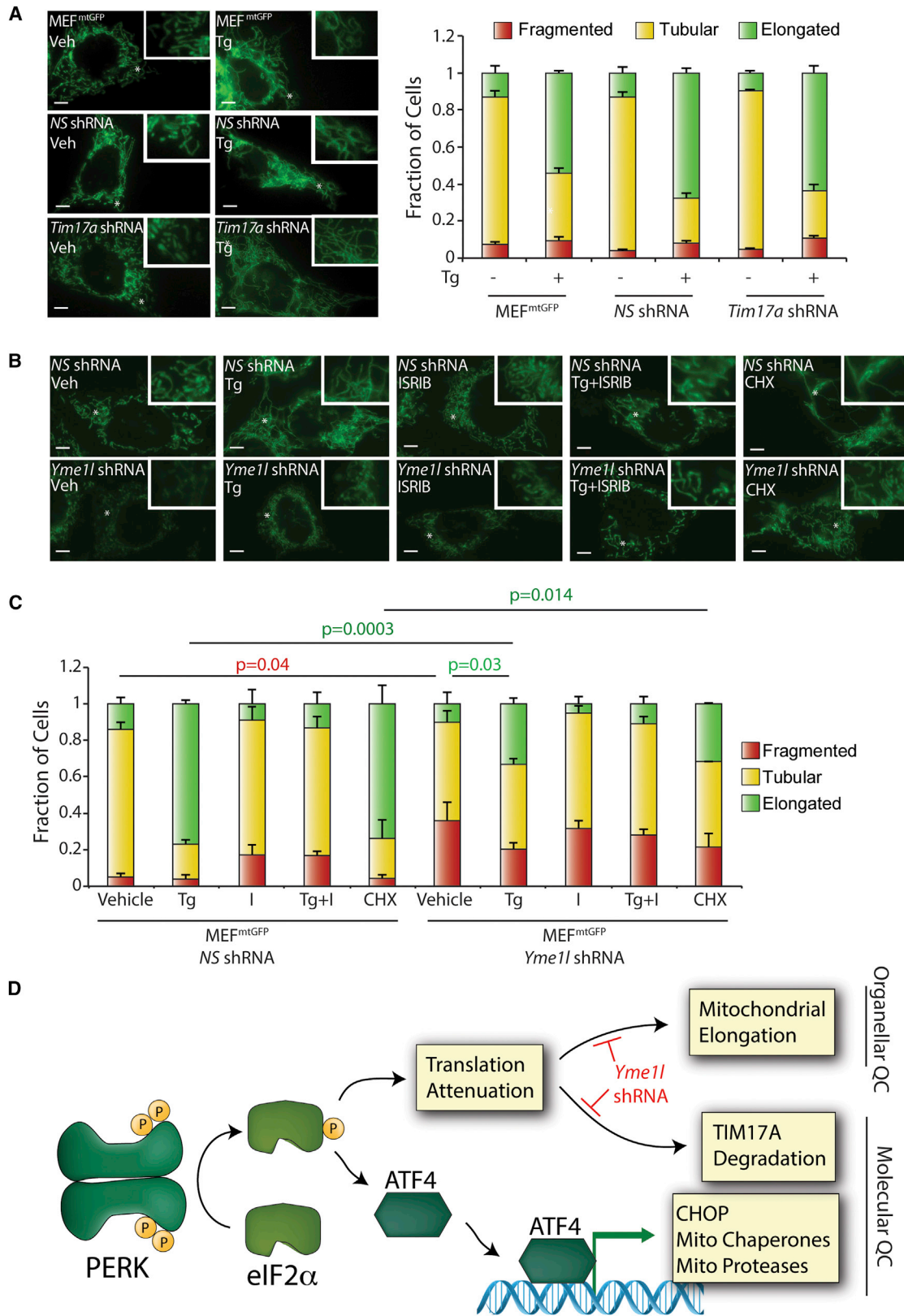
(F) Representative images of MEF^{WT}, *Perk*^{-/-}, *MEF* ^{$\Delta\Delta$} , and *Atf4*^{-/-} cells transiently transfected with mitochondrial-targeted GFP and treated for 6 hr with Tg (500 nM) or CHX (50 μ g/mL), as indicated. Scale bars, 5 μ m.

(Rainbolt et al., 2013). ER-stress-induced SIMH is also inhibited in *Perk*^{-/-} and *MEF* ^{$\Delta\Delta$} cells, further demonstrating that ER-stress-dependent SIMH requires PERK-regulated eIF2 α phosphorylation (Figure 2F).

Next, we determined the importance of PERK-regulated transcriptional signaling for ER-stress-dependent SIMH using *Atf4*^{-/-} MEFs deficient in the primary upstream PERK-regulated

transcription factor ATF4 (Harding et al., 2003). These cells show deficiencies in the transcriptional induction of PERK-regulated genes but not in translation attenuation induced by eIF2 α phosphorylation (Figure 2A). As such, Tg-dependent induction of *Lon*, *Hspa9*, and *Chop* is inhibited in *Atf4*^{-/-} cells (Figure S2J), while TIM17A degradation is not affected (Figure S2K). Interestingly, Tg-induced mitochondrial elongation is

not inhibited in *Atf4*^{-/-} MEFs (Figure 2F). This indicates that PERK-regulated SIMH does not require ATF4 transcriptional activity. The aforementioned results show that ER stress induces SIMH through a mechanism dependent on PERK-dependent eIF2 α phosphorylation but not ATF4. This suggests that PERK promotes SIMH downstream of eIF2 α phosphorylation-dependent



(legend on next page)

translation attenuation. Consistent with this, inhibiting translation in *Perk*^{-/-} and *MEF*^{ΔA} cells using CHX increases mitochondrial elongation in both genotypes (Figure 2F). This indicates that ER-stress-dependent SIMH is regulated by the PERK signaling arm of the UPR and activated by eIF2 α phosphorylation-dependent translation attenuation.

Yme1 Depletion Attenuates ER-Stress-Dependent Increases in Elongated Mitochondria

A key question emerging from the aforementioned results is, “How does PERK-dependent translational attenuation regulate SIMH?” Mitochondrial hyperfusion can be induced by diverse mechanisms, including protein kinase A (PKA)-dependent phosphorylation of the pro-fission GTPase DRP1 at position S637 (Gomes et al., 2011), reductions in total DRP1 protein levels (Sabouny et al., 2017), or HDAC6-dependent deacetylation of the outer membrane pro-fusion GTPase MFN1 (Lee et al., 2014). However, Tg treatment does not increase S637 phosphorylation or decrease total DRP1 levels in *Slp2*^{+/+} or *Slp2*^{-/-} MEFs (Figure S3A). Furthermore, co-addition of the PKA inhibitor KT5720 does not inhibit Tg-induced mitochondrial elongation in *MEF*^{mtGFP} cells (Figure S3B). Similarly, the addition of tubacin—an HDAC6 inhibitor (Haggarty et al., 2003)—does not reduce Tg-dependent mitochondrial elongation (Figure S3C). We also do not observe increased stability of the MFN1 or MFN2 outer membrane GTPases or processing of the inner membrane GTPase OPA1 in Tg-treated cells (Figure S3A)—two stress-responsive posttranslational modifications that can influence mitochondrial morphology (Chan, 2012; Shutt and McBride, 2013; Wai and Langer, 2016). These results suggest that PERK-regulated SIMH is induced through a mechanism different from those discussed above.

Apart from promoting SIMH, PERK-regulated translational attenuation reduces mitochondrial protein import through the degradation of the TIM23 subunit TIM17A (Rainbolt et al., 2013). We defined the relationship between SIMH and TIM17A degradation in *MEF*^{mtGFP} cells that were shRNA-depleted of *Tim17a* (Figures 3A and S3D). Depletion of *Tim17a* did not influence basal mitochondrial morphology or Tg-induced elongation in these cells, demonstrating that TIM17A degradation and SIMH are two distinct events induced by PERK-regulated translational attenuation.

TIM17A is degraded by the ATP-dependent inner membrane protease YME1L downstream of PERK-regulated translation attenuation (Rainbolt et al., 2013). YME1L also regulates inner membrane proteostasis and function through its assembly

into a complex with the inner membrane protease PARL and SLP2 (Wai et al., 2016), the latter being a protein whose depletion impairs ER-stress-dependent SIMH (Figures 1D–1G). Thus, we tested whether shRNA depletion of *Yme1* impairs mitochondrial elongation in response to ER stress. The depletion of *Yme1* in *MEF*^{mtGFP} inhibited Tg-dependent TIM17A degradation but did not influence PERK-dependent induction of LON, confirming efficient reduction in protease activity (Figures S3E and S3F). In the absence of stress, *Yme1*-depleted cells show increased mitochondrial fragmentation (Figures 3B and 3C), consistent with previous results (Anand et al., 2014; Mishra et al., 2014). Interestingly, *Yme1* depletion also reduced elongated mitochondria in Tg-treated cells, suggesting that YME1L is involved in ER-stress-dependent SIMH. In contrast, depletion of *Parl* does not influence Tg-dependent SIMH (Figures S3G and S3H).

Collectively, our results indicate that PERK regulates SIMH downstream of eIF2 α phosphorylation-dependent translational attenuation (Figure 3D). This PERK-regulated increase in mitochondrial elongation is independent of PERK-regulated TIM17A degradation but appears to involve the inner membrane protease YME1L, potentially reflecting the importance of degrading a short-lived mitochondrial protein in this process. We are currently focused on further defining the involvement of YME1L and, potentially, other proteases in regulating SIMH during ER stress.

Disruption of PERK-Regulated SIMH Increases Mitochondrial Fragmentation during ER Stress

SIMH suppresses premature fragmentation in response to diverse cellular insults (Chan, 2012; Shutt and McBride, 2013; Wai and Langer, 2016). Consistent with this, ISRIB-dependent inhibition of SIMH in *MEF*^{mtGFP} cells treated with Tg for 12 or 24 hr increased populations of fragmented mitochondria (Figures 4A and 4B). However, ISRIB inhibits both transcriptional and translational signaling induced by PERK (Figure 2A), preventing us from defining the specific contributions of PERK-regulated SIMH in protecting mitochondria from fragmentation. Therefore, we chose to further define the importance of SIMH in preventing premature ER-stress-induced fragmentation in *Slp2*^{-/-} MEFs, where PERK-dependent SIMH is inhibited (Figures 1D and 1E). Importantly, PERK-dependent transcriptional induction of *Lon*, *Hspa9*, and *Chop* (Figures S4A and S4B) and TIM17A degradation (induced by PERK-dependent translational attenuation; Figure S4C) are not affected in *Slp2*^{-/-} MEFs, demonstrating that PERK-dependent SIMH can be selectively

Figure 3. Yme1 Depletion Decreases Elongated Mitochondria during ER Stress

(A) Representative images and quantification of fragmented (red), tubular (yellow), or elongated (green) mitochondria in stable pools of *MEF*^{mtGFP} cells expressing non-silencing (NS) or *Tim17a* shRNA treated for 6 hr with thapsigargin (Tg; 500 nM). Uninfected *MEF*^{mtGFP} cells are also shown as a control. The inset shows a 2-fold magnification of the image centered at the asterisk. Scale bars, 5 μ m. Error bars indicate SEM from three independent experiments.

(B) Representative images of stable pools of *MEF*^{mtGFP} cells expressing non-silencing or *Yme1* shRNA treated for 6 hr with Tg. The inset shows a 2-fold magnification of the image centered at the asterisk. Scale bars, 5 μ m.

(C) Quantification of fragmented (red), tubular (yellow), or elongated (green) mitochondria in stable pools of *MEF*^{mtGFP} cells expressing non-silencing or *Yme1* shRNA treated for 6 hr with Tg (500 nM). Error bars indicate SEM from three independent experiments. p values for elongated (green text) or fragmented (red text) mitochondria from a two-tailed unpaired t test are shown.

(D) Illustration showing how PERK integrates transcriptional and translational signaling to coordinate mitochondria molecular and organellar quality control during ER stress. Genetic perturbations that disrupt these pathways are indicated in red.

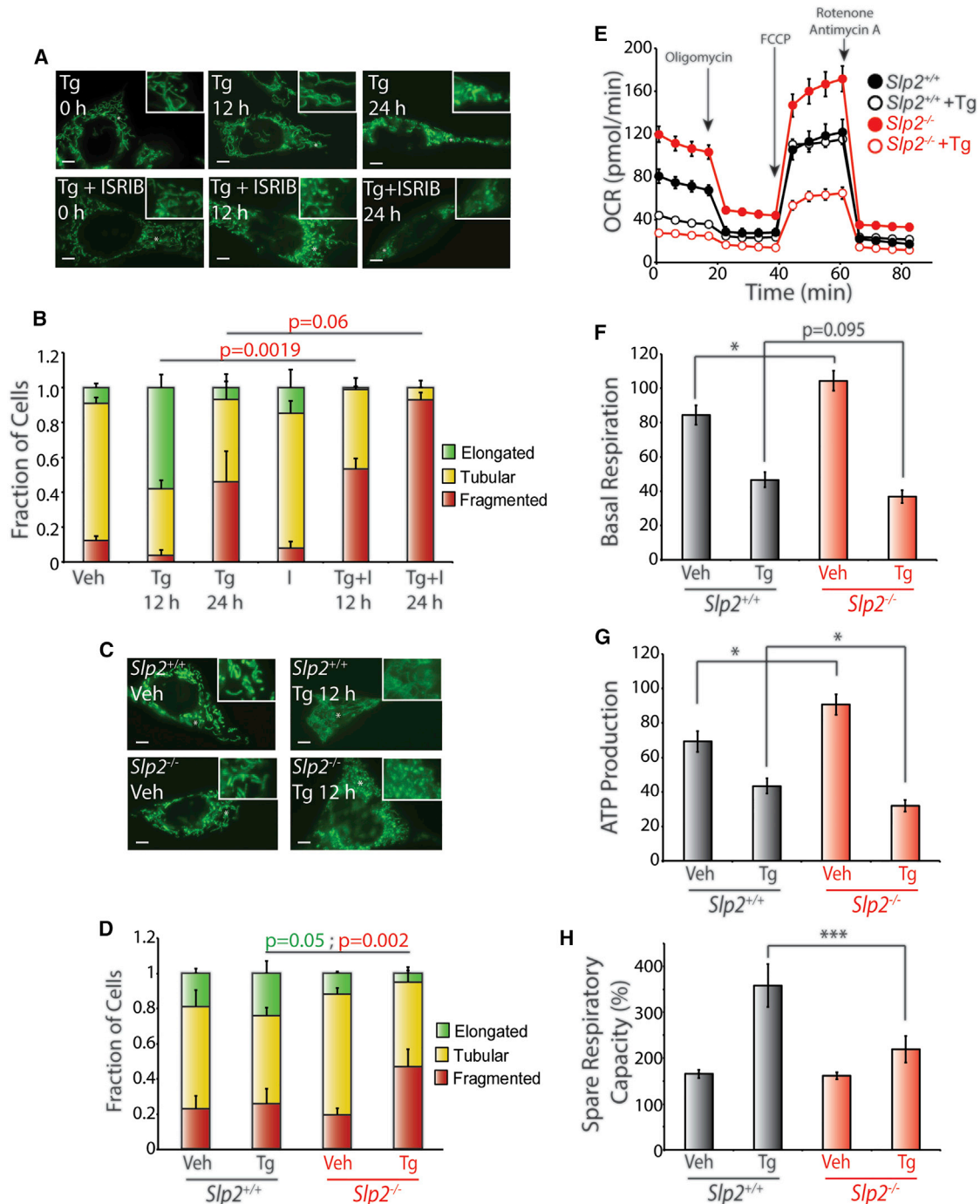


Figure 4. Pharmacologic or Genetic Inhibition of PERK-Regulated SIMH Disrupts ER-Stress-Dependent Regulation of Mitochondrial Morphology and Metabolism

(A) Representative images of MEF^{mtGFP} cells treated for 12 or 24 hr with thapsigargin (Tg; 500 nM) and/or ISRIB (200 nM), as indicated. The inset shows a 2-fold magnification of the image centered at the asterisk. Scale bars, 5 μ m.

(B) Quantification of fragmented (red), tubular (yellow), or elongated (green) mitochondria in MEF^{mtGFP} cells treated for 12 or 24 hr with Tg (500 nM) and/or ISRIB (200 nM). Error bars indicate SEM from three independent experiments. *p* values for fragmented mitochondria (red text) are shown for a one-tailed paired *t* test.

(C) Representative images of *Slp2*^{+/+} and *Slp2*^{-/-} MEF cells transiently transfected with mitochondrial-targeted GFP treated for 12 hr with Tg (500 nM). The inset shows a 2-fold magnification of the image centered at the asterisk. Scale bars, 5 μ m.

(D) Graph showing the fraction of *Slp2*^{+/+} and *Slp2*^{-/-} MEF cells transiently transfected with mtGFP containing fragmented (red), tubular (yellow), or elongated (green) mitochondria in cells treated for 12 hr with Tg (500 nM). Error bars indicate SEM for three independent experiments. *p* values for fragmented mitochondria (red text) are shown for a two-tailed paired *t* test.

(legend continued on next page)

inhibited in these cells. Interestingly, Tg treatment for 12 hr induces mitochondrial fragmentation in *Slp2*^{-/-} MEFs to extents similar to that observed in cells co-treated with Tg and ISRIB (Figures 4C and 4D). This indicates that PERK-regulated SIMH protects mitochondrial morphology and prevents premature fragmentation in response to ER stress.

The increased fragmentation observed in cells deficient in PERK-regulated SIMH could reflect increased sensitivity to ER insults. Consistent with this, pretreatment with Tg and ISRIB for 12 hr reduced the clonal expansion of MEF^{mtGFP} cells, as compared with cells pre-treated with Tg alone (Figure S4D). This is consistent with previous results and highlights that PERK signaling is important for dictating ER stress resistance (Sidrauski et al., 2013). However, we did not observe differences in the clonal expansion of *Slp2*^{+/+} and *Slp2*^{-/-} MEFs in this assay (Figure S4E). This likely reflects the importance of SLP2 in regulating apoptotic signaling through PARL-dependent processing of the pro-apoptotic Smac/Diablo (Saita et al., 2017). Consistent with this, *Slp2*^{-/-} MEFs show lower levels of active caspase 3 following Tg treatment (Figure S4F). Regardless, our results show that PERK-dependent SIMH protects mitochondria from premature fragmentation and could contribute to decrease cellular sensitivity to ER stress.

Slp2 Deficiency Decreases Mitochondrial Respiratory Chain Capacity during ER Stress

SIMH has been shown to promote mitochondrial metabolic activity in response to other types of stress (Tondera et al., 2009). We used the Seahorse extracellular flux assay to define how SLP2-dependent SIMH impacts mitochondria metabolic activity in response to ER stress. The serum-free conditions required for this experiment induce a mild increase in eIF2 α phosphorylation (Figure S4G), which is consistent with previous results showing that reduced serum promotes eIF2 α phosphorylation through a mechanism involving the alternative eIF2 α kinase GCN2 (Taniuchi et al., 2016). While this mild eIF2 α phosphorylation complicates the use of pharmacologic agents to block PERK signaling (e.g., ISRIB), we were able to monitor how ER stress influenced mitochondrial respiration in *Slp2*^{-/-} MEFs, where PERK-regulated SIMH is selectively inhibited. In the absence of stress, *Slp2*^{-/-} MEFs showed modest increases in basal respiration and ATP-linked respiration, as compared to *Slp2*^{+/+} controls (Figures 4E–4G). Pretreatment with Tg for 6 hr induced a significant reduction in these aspects of mitochondrial respiration in both *Slp2*^{+/+} and *Slp2*^{-/-} cells. However, this reduction was greater in *Slp2*^{-/-} MEFs, indicating that Tg differentially impacted mitochondrial metabolic activity in these cells. Similar results were observed upon Tm treatment (Figures S4H–S4J). Interestingly, the differential ER-stress-dependent decrease in basal and ATP-linked respiration in *Slp2*^{-/-} MEFs corresponded

with lower levels of spare respiratory capacity in these cells, as compared to *Slp2*^{+/+} controls (Figure 4H; Figure S4K). These results demonstrate that ER stress differentially impacts mitochondrial metabolic activity in *Slp2*^{-/-} cells deficient in ER-stress-induced SIMH and is consistent with previous results showing that SLP2-dependent SIMH promotes mitochondria metabolic activity (Tondera et al., 2009).

DISCUSSION

Here, we show that cells regulate mitochondrial morphology in response to acute ER stress by promoting protective SIMH through a mechanism involving translational attenuation induced by PERK-dependent eIF2 α phosphorylation (Figure 3D). PERK integrates transcriptional and translational signaling to remodel quality control pathways involved in protein import, folding, and proteolysis. Our results expand the scope of PERK's role in adapting mitochondria during ER stress by demonstrating that PERK signaling coordinates the regulation of both mitochondrial molecular quality control and morphology (i.e., organellar quality control). This coordination provides a unique platform to sensitively regulate mitochondria in response to diverse types of ER insults. PERK-dependent remodeling of molecular quality control pathways increases mitochondrial proteostasis capacity to promote proteome integrity and prevent the potentially pathologic accumulation of misfolded or damaged proteins within mitochondria during ER stress (Rainbolt et al., 2014). Our results indicate that PERK-dependent SIMH complements this regulation of mitochondrial molecular quality control by preventing premature mitochondrial fragmentation and promoting mitochondrial metabolic activity. By protecting these aspects of mitochondrial biology, PERK-regulated SIMH increases cellular energetic capacity to facilitate recovery following acute ER insults. Thus, the coordination of mitochondrial molecular and organellar quality control afforded by PERK activity demonstrates that this UPR signaling pathway is a key determinant in regulating mitochondrial function in response to ER stress.

The importance of PERK for regulating both molecular and organellar quality control indicates that alterations in PERK signaling could significantly influence mitochondrial function in disease states. Consistent with this, altered PERK activity is implicated in diverse diseases associated with mitochondrial dysfunction, including cardiovascular disorders, neurodegenerative diseases, and mitochondrialopathies such as Leber's hereditary optic neuropathy (LHON) (Brooks et al., 2014; Cortopassi et al., 2006; Freeman and Mallucci, 2016; Hetz and Mollereau, 2014; Liu and Dudley, 2015; Silva et al., 2009). Mutations in PERK implicated in Wolcott-Rallison syndrome are also suggested to induce pathologic mitochondrial dysfunction (Collardeau-Frachon et al., 2015; Engelmann et al., 2008; Søvik

(E) Representative plot of oxygen consumption rates (OCRs) for *Slp2*^{+/+} and *Slp2*^{-/-} MEFs pre-treated with Tg (500 nM) for 6 hr prior to analysis by Seahorse. (F) Graph showing basal respiration for *Slp2*^{+/+} and *Slp2*^{-/-} MEFs treated with Tg (500 nM) for 6 hr before OCR measurements. Error bars indicate SEM for n = 30, collected across three independent experiments. *p < 0.05 for a two-tailed unpaired t test.

(G) Graph showing ATP production of *Slp2*^{+/+} and *Slp2*^{-/-} MEFs treated with Tg (500 nM) for 6 hr before OCR measurements. Error bars indicate SEM for n = 30, collected across three independent experiments. *p < 0.05 for a two-tailed unpaired t test.

(H) Graph showing spare respiratory capacity of *Slp2*^{+/+} and *Slp2*^{-/-} MEFs treated with Tg (500 nM) for 6 hr before OCR measurements. Error bars indicate SEM for n = 30, collected across three independent experiments. ***p < 0.005 for a two-tailed unpaired t test.

et al., 2008). Aging-dependent alterations in PERK activity (Brown and Naidoo, 2012; Taylor, 2016) could also decrease cellular capacity to regulate mitochondria, potentially contributing to the pathologic mitochondrial dysfunction associated with aging-related diseases. Thus, our identification of PERK as a key stress-responsive signaling pathway involved in the coordinated regulation of mitochondria during ER stress provides a foundation to define the importance of altered PERK signaling in mitochondrial disease pathogenesis. In addition, our results indicate that therapeutic targeting of PERK signaling could provide a unique opportunity to ameliorate pathologic defects in mitochondria associated with diverse diseases.

EXPERIMENTAL PROCEDURES

Cell Culture and Plasmids

MEF^{mtGFP} (a kind gift from Peter Schultz, The Scripps Research Institute; TSRI) (Wang et al., 2012) and HeLa cells (purchased from the ATCC) were cultured in DMEM (Corning-Cellgro) supplemented with 10% fetal bovine serum (FBS; Omega Scientific), 2 mM L-glutamine (GIBCO), 100 U/mL⁻¹ penicillin, and 100 μg/mL⁻¹ streptomycin (GIBCO). MEF^{WT} and the *Slp2*^{+/+} and *Slp2*^{-/-} MEFs (a kind gift from Joaquin Madrenas, McGill University) (Mitsopoulos et al., 2015) were cultured as described earlier and supplemented with non-essential amino acids (GIBCO). *Perk*^{+/+}, *Perk*^{-/-}, MEF^{ΔA}, *Atf4*^{+/+}, and *Atf4*^{-/-} cells (kind gifts from Jonathan Lin) were cultured as described earlier and supplemented with non-essential amino acids and 55 μM 2-mercaptoethanol. Cells were maintained at 37°C and 5% CO₂. MEF cells were transfected with MEF Avalanche Transfection Reagent (EZ Biosystems) according to the manufacturer's protocol. Stable pools of cells expressing non-silencing or gene-specific knockdowns were generated through selection with puromycin (3 μg/mL⁻¹). HeLa cells were transfected by the calcium phosphate co-precipitation method. *SLP2*, *Tim17a*, *Yme1*, and *Parl* shRNA in pLKO.1 vector were obtained from Sigma. Stable pools of cells expressing non-silencing or gene-specific knockdowns were generated through selection with puromycin (3 μg/mL⁻¹ for MEF and 1 μg/mL⁻¹ for HeLa).

Fluorescence Microscopy and Mitochondria Scoring

Cells were seeded the day before on glass-bottom dishes coated with poly-D-lysine (Sigma) to reach a confluence of 50% the day of the experiment. Cells were treated in media with reagents for the indicated time and then washed 3 times with HBSS containing 10% FBS, 100 U/mL⁻¹ penicillin, and 100 μg/mL⁻¹ streptomycin and put in the same buffer for imaging. Images were then recorded with an Olympus IX71 microscope with 60× oil objective (Olympus), a Hamamatsu C8484 camera (Hamamatsu Photonics), and HCLImage software (Hamamatsu Photonics). For quantification, we collected images for more than 30 cells per condition and then blinded these images. Three researchers then scored the cells for containing primarily fragmented, tubular, or elongated mitochondria (see Figure S1A for examples of scoring). The scores from the three researchers were then averaged and combined with other independent experiments in the data presented in the bar graphs shown throughout the paper.

Statistical Analysis

Data are presented as mean ± SEM and were analyzed by paired one- or two-tailed (as indicated) Student's *t* test to determine significance. A one-tailed *t* test was used when a specific result could be predicted from published reports.

Additional materials and methods are described in the Supplemental Information.

SUPPLEMENTAL INFORMATION

Supplemental Information includes Supplemental Experimental Procedures and four figures and can be found with this article online at <https://doi.org/10.1016/j.celrep.2018.02.055>.

ACKNOWLEDGMENTS

We thank T. Kelly Rainbolt for intellectual contributions, experimental support, and critical reading of the manuscript. We thank Danling Wang and Peter Schultz (The Scripps Research Institute [TSRI]) for providing MEF^{mtGFP} cells; Jonathan Lin (UCSD) for providing *Perk*^{+/+}, *Perk*^{-/-}, MEF^{WT}, MEF^{ΔA}, *Atf4*^{+/+}, and *Atf4*^{-/-} MEFs; and Joaquin Madrenas (McGill University) for providing the *Slp2*^{+/+} and *Slp2*^{-/-} MEFs. We thank Peter Walter (UCSF) for providing the ATF6 inhibitor Ceapin. This work was supported by the NIH (NS095892 to R.L.W.). J.L. was supported by a George E. Hewitt Foundation postdoctoral fellowship.

AUTHOR CONTRIBUTIONS

J.L., J.M.S., V.W.R.M., A.M., and R.L.W. conceived, designed, performed, and interpreted the experiments. N.M. and M.C.A. performed experiments. R.L.W. supervised the project. All authors were involved in the drafting and revision of the manuscript.

DECLARATION OF INTERESTS

The authors declare no competing interests.

Received: September 20, 2017

Revised: January 5, 2018

Accepted: February 13, 2018

Published: March 13, 2018

REFERENCES

- Anand, R., Wai, T., Baker, M.J., Kladt, N., Schauss, A.C., Rugarli, E., and Langer, T. (2014). The i-AAA protease YME1L and OMA1 cleave OPA1 to balance mitochondrial fusion and fission. *J. Cell Biol.* 204, 919–929.
- Axten, J.M., Romeril, S.P., Shu, A., Ralph, J., Medina, J.R., Feng, Y., Li, W.H., Grant, S.W., Heerding, D.A., Minthorn, E., et al. (2013). Discovery of GSK2656157: an optimized PERK inhibitor selected for preclinical development. *ACS Med. Chem. Lett.* 4, 964–968.
- Baker, M.J., Tatsuta, T., and Langer, T. (2011). Quality control of mitochondrial proteostasis. *Cold Spring Harb. Perspect. Biol.* 3, a007559.
- Brooks, A.C., Guo, Y., Singh, M., McCracken, J., Xuan, Y.T., Srivastava, S., Bolli, R., and Bhatnagar, A. (2014). Endoplasmic reticulum stress-dependent activation of ATF3 mediates the late phase of ischemic preconditioning. *J. Mol. Cell. Cardiol.* 76, 138–147.
- Brown, M.K., and Naidoo, N. (2012). The endoplasmic reticulum stress response in aging and age-related diseases. *Front. Physiol.* 3, 263.
- Chan, D.C. (2012). Fusion and fission: interlinked processes critical for mitochondrial health. *Annu. Rev. Genet.* 46, 265–287.
- Collardeau-Frachon, S., Vasiljevic, A., Jouvét, A., Bouvier, R., Senée, V., and Nicolino, M. (2015). Microscopic and ultrastructural features in Wolcott-Rallison syndrome, a permanent neonatal diabetes mellitus: about two autopsy cases. *Pediatr. Diabetes* 16, 510–520.
- Cortopassi, G., Danielson, S., Alemi, M., Zhan, S.S., Tong, W., Carelli, V., Martinuzzi, A., Marzuki, S., Majamaa, K., and Wong, A. (2006). Mitochondrial disease activates transcripts of the unfolded protein response and cell cycle and inhibits vesicular secretion and oligodendrocyte-specific transcripts. *Mitochondrion* 6, 161–175.
- Cross, B.C., Bond, P.J., Sadowski, P.G., Jha, B.K., Zak, J., Goodman, J.M., Silverman, R.H., Neubert, T.A., Baxendale, I.R., Ron, D., and Harding, H.P. (2012). The molecular basis for selective inhibition of unconventional mRNA splicing by an IRE1-binding small molecule. *Proc. Natl. Acad. Sci. USA* 109, E869–E878.
- De Strooper, B., and Scorrano, L. (2012). Close encounter: mitochondria, endoplasmic reticulum and Alzheimer's disease. *EMBO J.* 31, 4095–4097.

- Doroudgar, S., and Glembotski, C.C. (2013). New concepts of endoplasmic reticulum function in the heart: programmed to conserve. *J. Mol. Cell. Cardiol.* **55**, 85–91.
- Engelmann, G., Meyburg, J., Shahbek, N., Al-Ali, M., Hairetis, M.H., Baker, A.J., Rodenburg, R.J., Wenning, D., Flechtenmacher, C., Ellard, S., et al. (2008). Recurrent acute liver failure and mitochondriopathy in a case of Wolcott-Rallison syndrome. *J. Inherit. Metab. Dis.* **31**, 540–546.
- Freeman, O.J., and Mallucci, G.R. (2016). The UPR and synaptic dysfunction in neurodegeneration. *Brain Res.* **1648** (Pt B), 530–537.
- Gallagher, C.M., and Walter, P. (2016). Ceapins inhibit ATF6 α signaling by selectively preventing transport of ATF6 α to the Golgi apparatus during ER stress. *eLife* **5**, e11880.
- Gallagher, C.M., Garri, C., Cain, E.L., Ang, K.K., Wilson, C.G., Chen, S., Hearn, B.R., Jaishankar, P., Aranda-Diaz, A., Arkin, M.R., et al. (2016). Ceapins are a new class of unfolded protein response inhibitors, selectively targeting the ATF6 α branch. *eLife* **5**, e11878.
- Gomes, L.C., Di Benedetto, G., and Scorrano, L. (2011). During autophagy mitochondria elongate, are spared from degradation and sustain cell viability. *Nat. Cell Biol.* **13**, 589–598.
- Haggarty, S.J., Koeller, K.M., Wong, J.C., Grozinger, C.M., and Schreiber, S.L. (2003). Domain-selective small-molecule inhibitor of histone deacetylase 6 (HDAC6)-mediated tubulin deacetylation. *Proc. Natl. Acad. Sci. USA* **100**, 4389–4394.
- Han, J., Back, S.H., Hur, J., Lin, Y.H., Gildersleeve, R., Shan, J., Yuan, C.L., Krokowski, D., Wang, S., Hatzoglou, M., et al. (2013). ER-stress-induced transcriptional regulation increases protein synthesis leading to cell death. *Nat. Cell Biol.* **15**, 481–490.
- Harding, H.P., Zhang, Y., Bertolotti, A., Zeng, H., and Ron, D. (2000). Perk is essential for translational regulation and cell survival during the unfolded protein response. *Mol. Cell* **5**, 897–904.
- Harding, H.P., Zhang, Y., Zeng, H., Novoa, I., Lu, P.D., Calfon, M., Sadri, N., Yun, C., Popko, B., Paules, R., et al. (2003). An integrated stress response regulates amino acid metabolism and resistance to oxidative stress. *Mol. Cell* **11**, 619–633.
- Hetz, C., and Mollereau, B. (2014). Disturbance of endoplasmic reticulum proteostasis in neurodegenerative diseases. *Nat. Rev. Neurosci.* **15**, 233–249.
- Hom, J.R., Gewandter, J.S., Michael, L., Sheu, S.S., and Yoon, Y. (2007). Thapsigargin induces biphasic fragmentation of mitochondria through calcium-mediated mitochondrial fission and apoptosis. *J. Cell. Physiol.* **212**, 498–508.
- Hori, O., Ichinoda, F., Tamatani, T., Yamaguchi, A., Sato, N., Ozawa, K., Kitao, Y., Miyazaki, M., Harding, H.P., Ron, D., et al. (2002). Transmission of cell stress from endoplasmic reticulum to mitochondria: enhanced expression of Lon protease. *J. Cell Biol.* **157**, 1151–1160.
- Lee, J.Y., Kapur, M., Li, M., Choi, M.C., Choi, S., Kim, H.J., Kim, I., Lee, E., Taylor, J.P., and Yao, T.P. (2014). MFN1 deacetylation activates adaptive mitochondrial fusion and protects metabolically challenged mitochondria. *J. Cell Sci.* **127**, 4954–4963.
- Liu, M., and Dudley, S.C., Jr. (2015). Role for the unfolded protein response in heart disease and cardiac arrhythmias. *Int. J. Mol. Sci.* **17**, 52.
- Malhotra, J.D., and Kaufman, R.J. (2011). ER stress and its functional link to mitochondria: role in cell survival and death. *Cold Spring Harb. Perspect. Biol.* **3**, a004424.
- Mercado, G., Valdés, P., and Hetz, C. (2013). An ERcentric view of Parkinson's disease. *Trends Mol. Med.* **19**, 165–175.
- Mishra, P., Carelli, V., Manfredi, G., and Chan, D.C. (2014). Proteolytic cleavage of Opa1 stimulates mitochondrial inner membrane fusion and couples fusion to oxidative phosphorylation. *Cell Metab.* **19**, 630–641.
- Mitsopoulos, P., Chang, Y.H., Wai, T., König, T., Dunn, S.D., Langer, T., and Madrenas, J. (2015). Stomatin-like protein 2 is required for in vivo mitochondrial respiratory chain supercomplex formation and optimal cell function. *Mol. Cell Biol.* **35**, 1838–1847.
- Prell, T., Lautenschläger, J., and Grosskreutz, J. (2013). Calcium-dependent protein folding in amyotrophic lateral sclerosis. *Cell Calcium* **54**, 132–143.
- Quirós, P.M., Langer, T., and López-Otín, C. (2015). New roles for mitochondrial proteases in health, ageing and disease. *Nat. Rev. Mol. Cell Biol.* **16**, 345–359.
- Rainbolt, T.K., Atanassova, N., Genereux, J.C., and Wiseman, R.L. (2013). Stress-regulated translational attenuation adapts mitochondrial protein import through Tim17A degradation. *Cell Metab.* **18**, 908–919.
- Rainbolt, T.K., Saunders, J.M., and Wiseman, R.L. (2014). Stress-responsive regulation of mitochondria through the ER unfolded protein response. *Trends Endocrinol. Metab.* **25**, 528–537.
- Sabouny, R., Fraunberger, E., Geoffrion, M., Ng, A.C., Baird, S.D., Sreaton, R.A., Milne, R., McBride, H.M., and Shutt, T.E. (2017). The Keap1-Nrf2 stress response pathway promotes mitochondrial hyperfusion through degradation of the mitochondrial fission protein Drp1. *Antioxid. Redox Signal.* **27**, 1447–1459.
- Saita, S., Nolte, H., Fiedler, K.U., Kashkar, H., Venne, A.S., Zahedi, R.P., Krüger, M., and Langer, T. (2017). PARL mediates Smac proteolytic maturation in mitochondria to promote apoptosis. *Nat. Cell Biol.* **19**, 318–328.
- Scheuner, D., Song, B., McEwen, E., Liu, C., Laybutt, R., Gillespie, P., Saunders, T., Bonner-Weir, S., and Kaufman, R.J. (2001). Translational control is required for the unfolded protein response and in vivo glucose homeostasis. *Mol. Cell* **7**, 1165–1176.
- Shutt, T.E., and McBride, H.M. (2013). Staying cool in difficult times: mitochondrial dynamics, quality control and the stress response. *Biochim. Biophys. Acta* **1833**, 417–424.
- Sidrauski, C., Acosta-Alvear, D., Khoutorsky, A., Vedantham, P., Hearn, B.R., Li, H., Gamache, K., Gallagher, C.M., Ang, K.K., Wilson, C., et al. (2013). Pharmacological brake-release of mRNA translation enhances cognitive memory. *eLife* **2**, e00498.
- Silva, J.M., Wong, A., Carelli, V., and Cortopassi, G.A. (2009). Inhibition of mitochondrial function induces an integrated stress response in oligodendroglia. *Neurobiol. Dis.* **34**, 357–365.
- Søvik, O., Njølstad, P.R., Jellum, E., and Molven, A. (2008). Wolcott-Rallison syndrome with 3-hydroxydicarboxylic aciduria and lethal outcome. *J. Inherit. Metab. Dis.* **31** (Suppl 2), S293–S297.
- Taniuchi, S., Miyake, M., Tsugawa, K., Oyadomari, M., and Oyadomari, S. (2016). Integrated stress response of vertebrates is regulated by four eIF2 α kinases. *Sci. Rep.* **6**, 32886.
- Taylor, R.C. (2016). Aging and the UPR(ER). *Brain Res.* **1648** (Pt B), 588–593.
- Tondera, D., Grandemange, S., Jourdain, A., Karbowski, M., Mattenberger, Y., Herzog, S., Da Cruz, S., Clerc, P., Raschke, I., Merkwirth, C., et al. (2009). SLP-2 is required for stress-induced mitochondrial hyperfusion. *EMBO J.* **28**, 1589–1600.
- Vannuvel, K., Renard, P., Raes, M., and Arnould, T. (2013). Functional and morphological impact of ER stress on mitochondria. *J. Cell. Physiol.* **228**, 1802–1818.
- Verdejo, H.E., del Campo, A., Troncoso, R., Gutierrez, T., Toro, B., Quiroga, C., Pedrozo, Z., Munoz, J.P., Garcia, L., Castro, P.F., and Lavandero, S. (2012). Mitochondria, myocardial remodeling, and cardiovascular disease. *Curr. Hypertens. Rep.* **14**, 532–539.
- Wai, T., and Langer, T. (2016). Mitochondrial dynamics and metabolic regulation. *Trends Endocrinol. Metab.* **27**, 105–117.
- Wai, T., Saita, S., Nolte, H., Müller, S., König, T., Richter-Dennerlein, R., Sprenger, H.G., Madrenas, J., Mühlmeister, M., Brandt, U., et al. (2016). The membrane scaffold SLP2 anchors a proteolytic hub in mitochondria containing PARL and the i-AAA protease YME1L. *EMBO Rep.* **17**, 1844–1856.
- Walter, P., and Ron, D. (2011). The unfolded protein response: from stress pathway to homeostatic regulation. *Science* **334**, 1081–1086.
- Wang, D., Wang, J., Bonamy, G.M., Meeusen, S., Bruschi, R.G., Turk, C., Yang, P., and Schultz, P.G. (2012). A small molecule promotes mitochondrial fusion in mammalian cells. *Angew. Chem. Int. Ed. Engl.* **51**, 9302–9305.
- Wek, R.C., and Cavener, D.R. (2007). Translational control and the unfolded protein response. *Antioxid. Redox Signal.* **9**, 2357–2371.
- Youle, R.J., and Narendra, D.P. (2011). Mechanisms of mitophagy. *Nat. Rev. Mol. Cell Biol.* **12**, 9–14.

Cell Reports, Volume 22

Supplemental Information

The PERK Arm of the Unfolded Protein Response

Regulates Mitochondrial Morphology

during Acute Endoplasmic Reticulum Stress

Justine Lebeau, Jaclyn M. Saunders, Vivian W.R. Moraes, Aparajita Madhavan, Nicole Madrazo, Mary C. Anthony, and R. Luke Wiseman

SUPPLEMENTAL EXPERIMENTAL PROCEDURES

Plasmids and Reagents

The mitochondria GFP plasmid was constructed by incorporating GFP 3' to a CoxVII mitochondria targeting sequence and cloned between the BamHI and NotI sites in the pENTR1A Gateway entry vector. The ^{mt}GFP sequence was then incorporated into the pDEST40 Gateway destination plasmid by clonase recombination for use in our transfections. The following reagents were acquired from commercial sources and used following the manufacturer instructions: ISRIB (Sigma), Thapsigargin (AdipoGen), Tunicamycin (AG Scientific), cycloheximide (Alfa Aesar), GSK2656157 (BioVision), 4 μ 8c (EMD Millipore), Ceapin (a kind gift from Peter Walter), KT5720 (Santa Cruz), Tubacin (Sigma), Oligomycin (Sigma), FCCP (Sigma), Rotenone (Sigma) and Antimycin A (Sigma).

Gene	TRC number
<i>SLP2 (human)</i>	TRCN0000173985
	TRCN0000194539
<i>Tim17a (mouse)</i>	TRCN0000114221
<i>Yme1l (mouse)</i>	TRCN0000031201
<i>Parl (mouse)</i>	TRCN0000126236

Quantitative Polymerase Chain Reaction (qPCR)

The relative mRNA expression levels of target genes were measured using quantitative RT-PCR. Cells were treated as described, washed with DBPS, and then RNA was extracted using the Quick-RNA MiniPrep Kit (Zymo Research). qPCR reactions were performed on cDNA prepared from 500 ng of total cellular RNA using the QuantiTect Reverse Transcription Kit (QIAGEN). The FastStart Universal SYBR Green Master Mix (Roche), cDNA, and appropriate primers purchased from Integrated DNA Technologies (see table) were used for amplifications (6 min at 95°C then 45 cycles of 10 s at 95°C, 30 s at 60°C) in an ABI 7900HT Fast Real Time PCR machine. Primer integrity was assessed by a thermal melt to confirm homogeneity and the absence of primer dimers. Transcripts were normalized to the housekeeping genes *Rplp2* and all measurements were performed in triplicate. Data were analyzed using the RQ Manager and DataAssist 2.0 softwares (ABI).

Primers used for qPCR

Name	Forward	Reverse
<i>Lon (mouse)</i>	5'-GGCAGCCTAGAGGTGACAGG-3'	5'-ATGCAGGTGGATGTGTGAGG-3'
<i>Hspa9 (mouse)</i>	5'-GTGCTGCTCCTGGATGTCAC-3'	5'-CATCTCTCGTTCCCCCTGAC-3'
<i>Chop (mouse)</i>	5'-GGAGCTGGAAGCCTGGTAG-3'	5'-TGTGCGTGTGACCTCTGTTG-3'
<i>Rplp2 (mouse)</i>	5'-TGTCATCGCTCAGGGTGTG-3'	5'-AAGCCAAATCCCATGTCGTC-3'
<i>Parl (mouse)</i>	5'-TTCACCATTGGGTTACAGG-3'	5'-TTTTGTGGCCGTATGCTGTC-3'
<i>Yme11 (mouse)</i>	5'-GGTGGAGGAAGCCAAACAAG-3'	5'-AGGGACGTCAGCTTCTCCTG-3'
<i>SLP2 (human)</i>	5'-AGGAGAGGCCAGTGCAGTTC-3'	5'-AGTCCTTGGCCAGTTTGGAG-3'
<i>Rplp2 (human)</i>	5'-CGTCGCCTCCTACCTGCT-3'	5'-CCATTCAGCTCACTGATAACCTTG-3'

Cellular Lysates and Immunoblotting

After treatments, cells were washed twice with DPBS, scraped and cell pellets were lysed with lysis buffer (20mM Hepes [pH 7.4], 100mM NaCl, 1mM EDTA, 1% Triton) containing a protease inhibitor cocktail (Roche). Total protein concentration in cellular lysates was normalized using Bio-Rad protein assay. Lysates were then denatured with 6X Laemmli buffer and boiled before being separated by SDS-PAGE. Samples were transferred onto nitrocellulose membranes (Bio-Rad) for immunoblotting and blocked with 5% milk in Tris Buffer Saline (w/v) following incubation overnight at 4°C with primary antibodies. Membranes were washed, incubated with IR-Dye conjugated secondary antibodies and analyzed using Odyssey Infrared Imaging System (LI-COR Biosciences). Quantification was carried out with LI-COR Image Studio software. Primary antibodies were acquired from commercial sources and used in the indicated dilutions in antibody buffer (50mM Tris [pH 7.5], 150mM NaCl supplemented with 5% BSA (w/v) and 0.1% NaN₃ (w/v): Tim17A (Thermo Scientific, 1:1000), Tim23 (BD Transduction Labs, 1:1000), HSP60 [LK1] (Thermo Scientific, 1:1000), Tubulin [B-5-1-2] (Sigma, 1:5000), OPA1 (BD Transduction Labs, 1:2000), SLP2 (ProteinTech, 1:1000), PS51-eif2 α (Cell Signaling, 1:1000), eif2 α (Cell Signaling, 1:1000), Lon (ProteinTech, 1:1000), P-Drp1 S637 (Cell Signaling, 1:1000), Drp-1 (BD Biosciences, 1:1000), MFN2 (Cell Signaling, 1:1000), MFN1 (Abcam, 1:1000), YME1L (Abgent, 1:1000), CHOP (Santa Cruz, 1:1000), Cleaved caspase 3 (Cell signaling, 1:1000).

[³⁵S] Metabolic labeling

Cells were metabolically labeled with 110 μ Ci/ml EasyTag Express³⁵S Protein Labeling Mix (PerkinElmer) in DMEM without cysteine and methionine (Corning-Cellgro) supplemented with 10% dialyzed FBS, 2mM L-glutamine, 100 U ml⁻¹ penicillin and 100 μ g ml⁻¹ streptomycin. After treatment as indicated, cells were washed and recovered in labeling media for 30min. Following labeling, whole cell lysates were prepared in RIPA buffer (50mM Tris [pH 7.5], 150mM NaCl, 1% Triton X100, 0.5% sodium deoxycholate, 0.1% SDS) containing proteases inhibitors cocktail (Roche). Samples were denatured with 6X Laemmli buffer, boiled and separated by SDS-PAGE. Gels were stained with Coomassie Blue, dried and imaged by autoradiography using a Typhoon Trio Imager (GE Healthcare).

Clonal expansion

Cells were treated for 12hrs and then washed, trypsinized and counted. Cells were seeded in three different dilutions containing 30,000, 15,000, and 10,000 cells and incubated for four days at 37°C. Crystal violet staining solution (0.5% crystal violet (w/v), 20% methanol) was added and samples were washed twice with PBS and three times with water. After drying overnight, quantification was performed by diluting crystals with 1ml sodium citrate solution (0.1M [pH 4.2], 50% methanol (v/v)) and absorbance was read at 550nm.

Mitochondrial Respiration measurements

Mitochondrial Respiration parameters were measured using a Mito Stress Test Kit and XF96 Extracellular Flux Analyzer (Seahorse Bioscience) according to the manufacturer's protocol. In brief, 15,000 cells were plated on Cell-Tak (Corning) coated wells in their standard growing media and cultured overnight. The next day, cells were treated with drugs and incubated at 37°C, 5%CO₂ for 6 h. Seahorse media (DMEM no red phenol, no bicarbonate, 25mM glucose, 1mM pyruvate, 2mM Glutamine, MEM Non-Essential Amino Acids, pH7.4) was used to wash the cells and measure oxygen consumption rate (OCR). The mito stress test was assayed according to the manufacturer's protocol. Briefly, each parameter was measured by 4 measurements every 5 min following injections of drugs. Basal respiration measurement was followed by Oligomycin (2 μ M), FCCP (0.5 μ M) and Rotenone/Antimycin (1 μ M each) injections. Parameters are represented as average of 3 independent experiments from 4 measurements of 10 wells per conditions. Spare respiratory capacity was calculated as a % of the ratio of the maximal to basal respiration.

SUPPLEMENTAL FIGURES

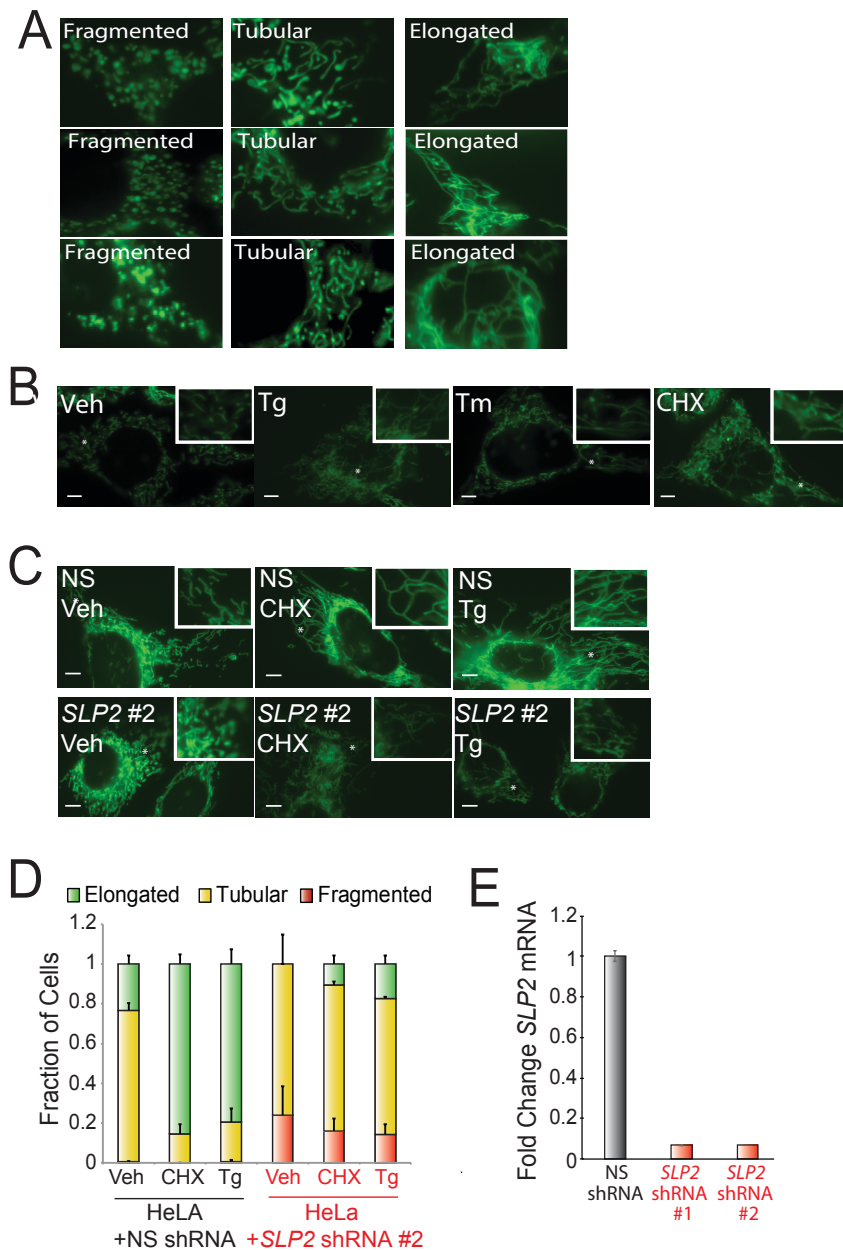


Figure S1 (Supplement to Figure 1)

- Representative images showing the fragmented, tubular, and elongated morphologies of MEF^{mtGFP} cells.
- Representative images of MEF^{mtGFP} cells treated for 6 h with thapsigargin (Tg; 500 nM), tunicamycin (Tm; 1 μ M), or cycloheximide (CHX; 50 μ g/mL). The inset shows a 2-fold magnification of the image centered at the *. Scale bar shows 5 μ m.
- Representative images of HeLa cells stably expressing non-silencing (NS) shRNA or *SLP2* shRNA #2 and transfected with mitochondria-targeted GFP. Cells were treated for 6 h with thapsigargin (Tg; 500 nM) or cycloheximide (CHX; 50 μ g/mL), as indicated. The inset shows a 2-fold magnification of the image centered at the *. Scale bar shows 5 μ m.
- Graph showing the fraction of HeLa cells stably expressing non-silencing (NS) shRNA or *SLP2* shRNA #2 and transfected with mitochondria-targeted GFP containing fragmented (red), tubular (yellow), or elongated (green) mitochondria following treatment for 6 h with thapsigargin (Tg; 500 nM), cycloheximide (CHX; 50 μ g/mL) or ISRIB (200 nM), as indicated. Error bars show SEM for two independent experiments. Representative images from these cells are shown in **Fig. S1C**.
- Graph showing the relative mRNA levels of *SLP2* in HeLa cells expressing non-silencing (NS) shRNA, *SLP2* shRNA #1 or *SLP2* shRNA #2, confirming depletion of *SLP2* in these cells. Data are normalized to cells expressing NS shRNA. Error bars show 95% confidence interval.

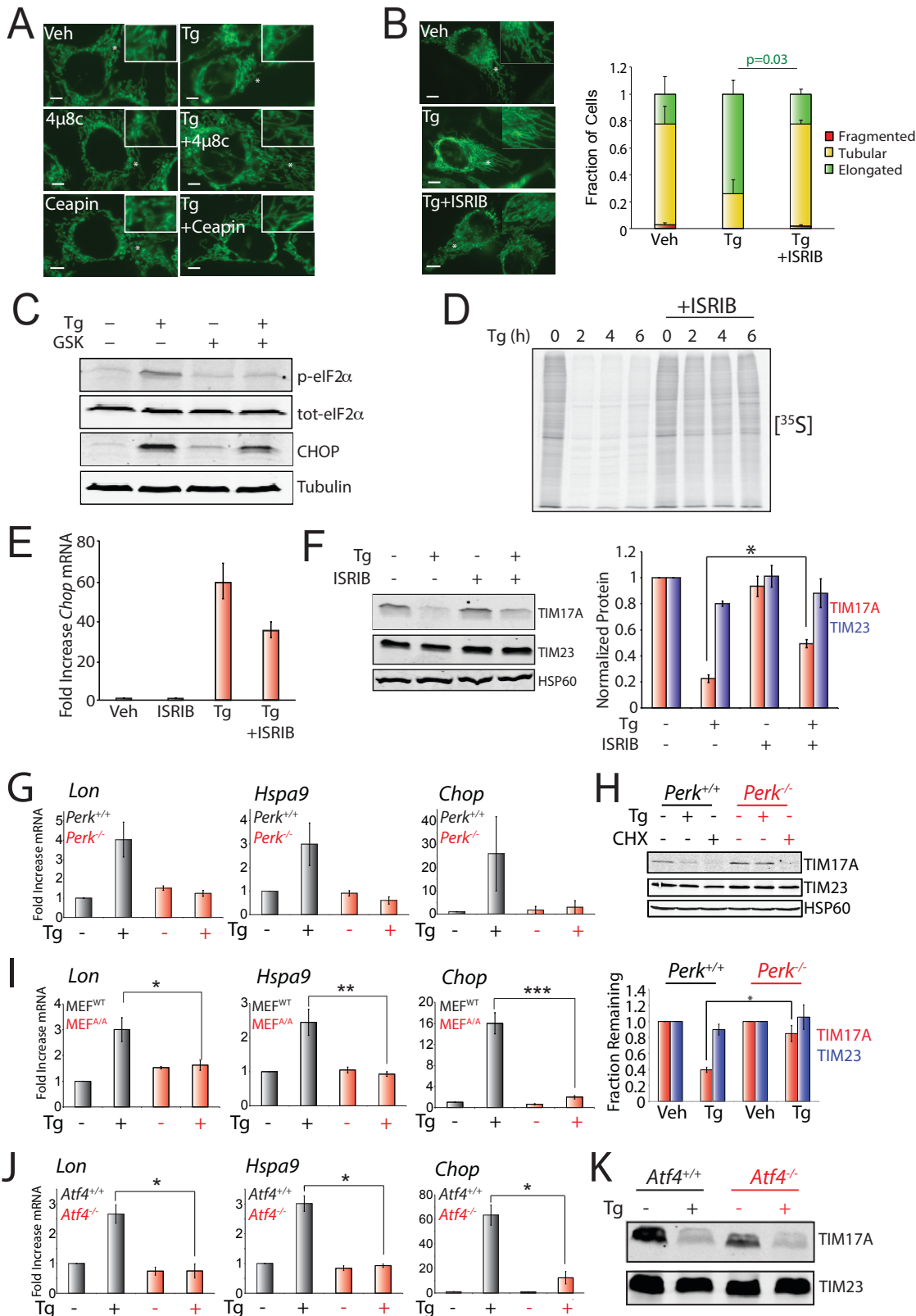


Figure S2 (Supplement to Figure 2)

- A.** Representative images of MEF^{mtGFP} cells treated for 6 h with thapsigargin (Tg; 500 nM), 4 μ 8c (an IRE1 inhibitor; 10 μ M) or Ceapin (an ATF6 inhibitor; 2.5 μ M), as indicated. The inset shows a 2-fold magnification of the image centered at the *. Scale bar shows 5 μ m.
- B.** Representative images and quantifications of HeLa cells transiently transfected with mitochondria-targeted GFP and treated for 6 h with thapsigargin (Tg; 500 nM) and/or ISRIB (200 nM). The inset shows a 2-fold magnification of the image centered at the *. Scale bar shows 5 μ m. Graph shows the fraction of HeLa cells containing fragmented (red), tubular (yellow), or elongated (green) mitochondria, as indicated. Error bars show SEM for three independent experiments. p-values shown for elongated (green text) mitochondria for a two-tailed paired t-test.

- C. Immunoblot of MEF^{mtGFP} cells treated for 6 h with thapsigargin (Tg; 500 nM) and/or GSK2656157 (GSK; 10 μM). Treatment with GSK2656157 reduces Tg-dependent eIF2a phosphorylation and CHOP expression, confirming that GSK2656157 inhibits PERK signaling during ER stress.
- D. Autoradiogram of lysates prepared from MEF^{WT} cells labeled with [³⁵S]-methionine for 15 min. Cells were pretreated with thapsigargin (Tg; 500 nM) and ISRIB (200 nM) for the indicated time prior to metabolic labeling. Treatment with ISRIB attenuates the Tg-dependent reduction in [³⁵S] incorporation demonstrating that ISRIB inhibits eIF2a-dependent translational signaling.
- E. Graph showing *Chop* expression in MEF^{WT} cells treated for 6 h with thapsigargin (Tg; 500 nM) and/or ISRIB (200 nM). Error bars show 95% confidence interval. Treatment with ISRIB decreases Tg-dependent increases in *Chop* expression, confirming that this compound attenuates PERK-dependent transcriptional signaling.
- F. Representative immunoblot and quantifications of TIM17A and TIM23 in lysates prepared from MEF^{WT} cells treated for 6 h with thapsigargin (Tg; 500 nM) and/or ISRIB (200 nM). Graph shows normalized TIM17A (red) or TIM23 (blue) protein levels relative to untreated controls. Error bars show SEM for three independent experiments. *p<0.05 from a two-tailed paired t-test. Treatment with ISRIB inhibits Tg-dependent TIM17A degradation induced by eIF2a-dependent translational attenuation, further confirming that this compound inhibits PERK signaling.
- G. Graph showing *Lon*, *Hspa9* and *Chop* mRNA levels in *Perk*^{+/+} (grey) or *Perk*^{-/-} (red) cells treated for 6 h with thapsigargin (Tg; 500 nM). Error bars show 95% confidence interval. The inhibition of the Tg-dependent induction of these genes in *Perk*^{-/-} MEFs confirms inhibition of PERK-regulated transcriptional signaling in these cells.
- H. Representative immunoblot and quantification of TIM17A (red) and TIM23 (blue) in lysates prepared from *Perk*^{+/+} and *Perk*^{-/-} cells treated with thapsigargin (500 nM; 6 h). Lysates prepared from *Perk*^{+/+} or *Perk*^{-/-} cells treated with cycloheximide (CHX; 50 μg/mL, 6 h) are shown as a control in the immunoblot. Graph shows normalized TIM17A (red) or TIM23 (blue) protein levels relative to untreated controls. Error bars show SEM for n=3. *p<0.05 for a two-tailed t-test. The inhibition of Tg-dependent Tim17A degradation in *Perk*^{-/-} MEFs confirms that PERK-regulated translational signaling is inhibited in these cells.
- I. Graph showing *Lon*, *Hspa9* and *Chop* mRNA levels in MEF^{WT} (grey) or MEF^{ΔΔ} (red) cells treated for 6 h with thapsigargin (Tg; 500 nM). Error bars show SEM for n=3 experiments. *p<0.05; **p<0.01, ***p<0.005 for a two-tailed paired t-test. The inhibition of the Tg-dependent induction of these genes in MEF^{ΔΔ} cells confirms inhibition of PERK-regulated transcriptional signaling in these cells.
- J. Graph showing *Lon*, *Hspa9* and *Chop* mRNA in *Atf4*^{+/+} (grey) or *Atf4*^{-/-} (red) cells treated for 6 h with thapsigargin (Tg; 500 nM). Error bars SEM for n=3 independent experiments. *p<0.05 for a two-tailed paired t-test. The inhibition of the Tg-dependent induction of these genes in *Atf4*^{-/-} MEFs confirms inhibition of PERK-regulated transcriptional signaling in these cells.
- K. Representative immunoblot of TIM17A in lysates prepared from *Atf4*^{+/+} and *Atf4*^{-/-} MEF cells treated for 6 h with or without thapsigargin (Tg; 500 nM). The efficient Tim17A degradation observed in *Atf4*^{-/-} MEFs confirms that PERK-regulated translational attenuation (required for Tim17A degradation) is not impaired in these cells.

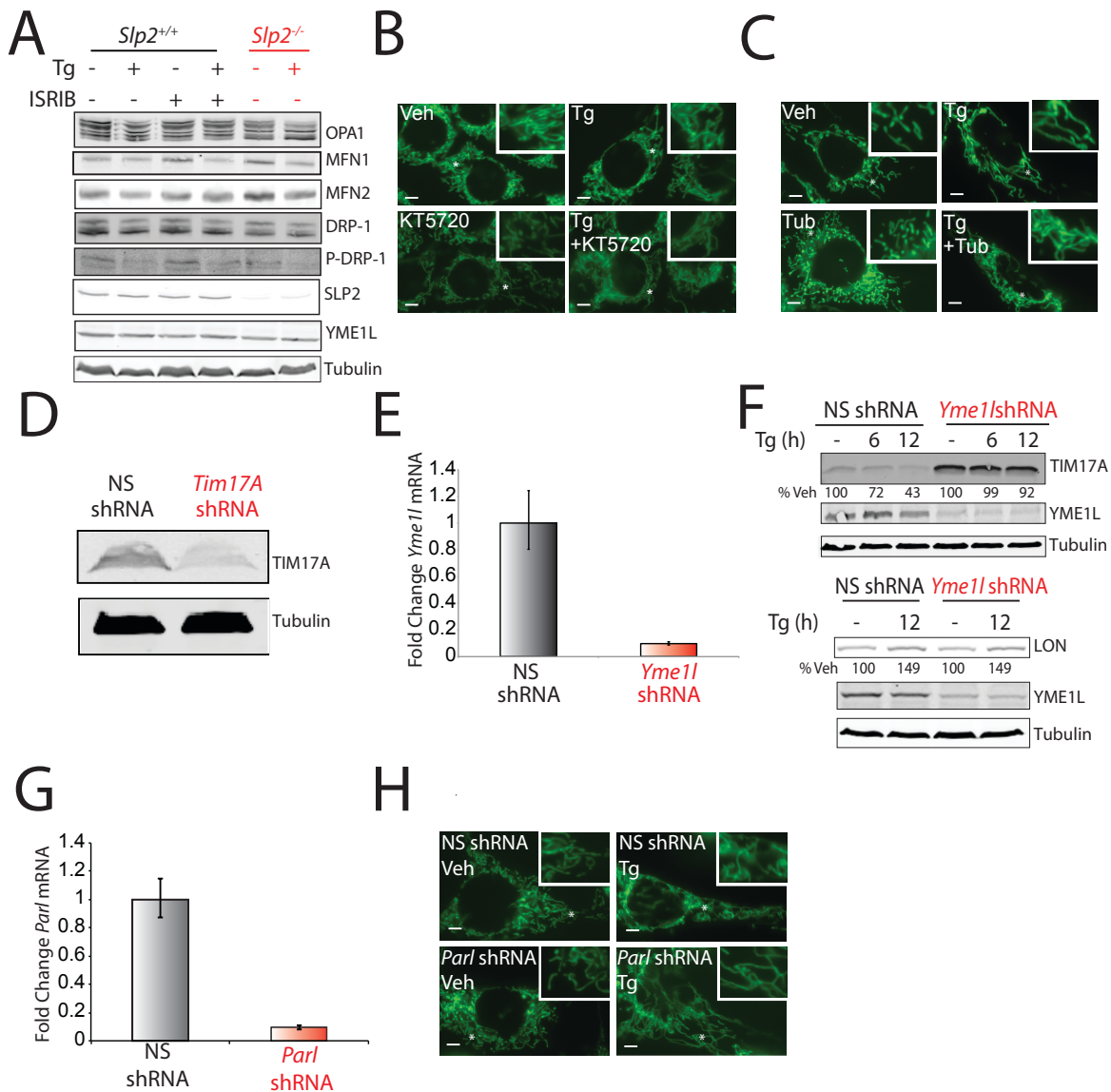


Figure S3 (Supplement to Figure 3)

- A.** Immunoblot of lysates prepared from *Slp2*^{+/+} and *Slp2*^{-/-} MEFs treated with thapsigargin (Tg; 500 nM) and/or ISRIB (200 nM) for 6 h, as indicated. Tg treatment does not significantly change OPA1 processing, total MFN2 or MFN1 protein levels, total DRP1 protein levels, or phosphorylation of DRP1 in an ISRIB or *Slp2*-dependent manner. This suggests that ER stress induced mitochondrial elongation, which is inhibited by ISRIB or *Slp2* depletion, proceeds through a mechanism independent of these posttranslational alterations of mitochondrial GTPases.
- B.** Representative fluorescence images of MEF^{mtGFP} cells treated with thapsigargin (Tg; 500 nM) and/or the PKA inhibitor KT5720 (1 μM) for 6h. The inset shows a 2-fold magnification of the image centered at the *. Scale bar shows 5 μm.
- C.** Representative fluorescence images of MEF^{mtGFP} cells treated with thapsigargin (Tg; 500 nM) and/or the HDAC6-inhibitor Tubacin (10 μM) for 6h. The inset shows a 2-fold magnification of the image centered at the *. Scale bar shows 5 μm.
- D.** Representative immunoblot of TIM17A from lysates prepared from MEF^{mtGFP} cells stably expressing non-silencing (NS) or *Tim17a* shRNA, confirming depletion of *Tim17a* in these cells.
- E.** Graph showing *Yme1l* mRNA in MEF^{mtGFP} cells stably expressing non-silencing (NS) or *Yme1l* shRNA, confirming depletion of *Yme1l* in these cells.
- F.** Representative immunoblot of TIM17A and LON from lysates prepared from MEF^{mtGFP} cells stably expressing non-silencing (NS) shRNA or *Yme1l* shRNA, treated for 6 or 12 h with thapsigargin (Tg; 500 nM). The impaired Tg-dependent degradation of Tim17A in these cells confirms reduced YME1L proteolytic activity. In contrast, the increase in LON protein levels in Tg-treated cells depleted of *Yme1l* shows that PERK-regulated signaling is not significantly impaired in these cells.
- G.** Graph showing *Parl* mRNA in MEF^{mtGFP} cells stably expressing non-silencing (NS) shRNA or *Parl* shRNA, confirming depletion of *Parl* in these cells.
- H.** Representative fluorescence images of MEF^{mtGFP} cells stably expressing non-silencing (NS) or *Parl* shRNA treated with thapsigargin (Tg; 500 nM) for 6h. The inset shows a 2-fold magnification of the image centered at the *. Scale bar shows 5 μm.

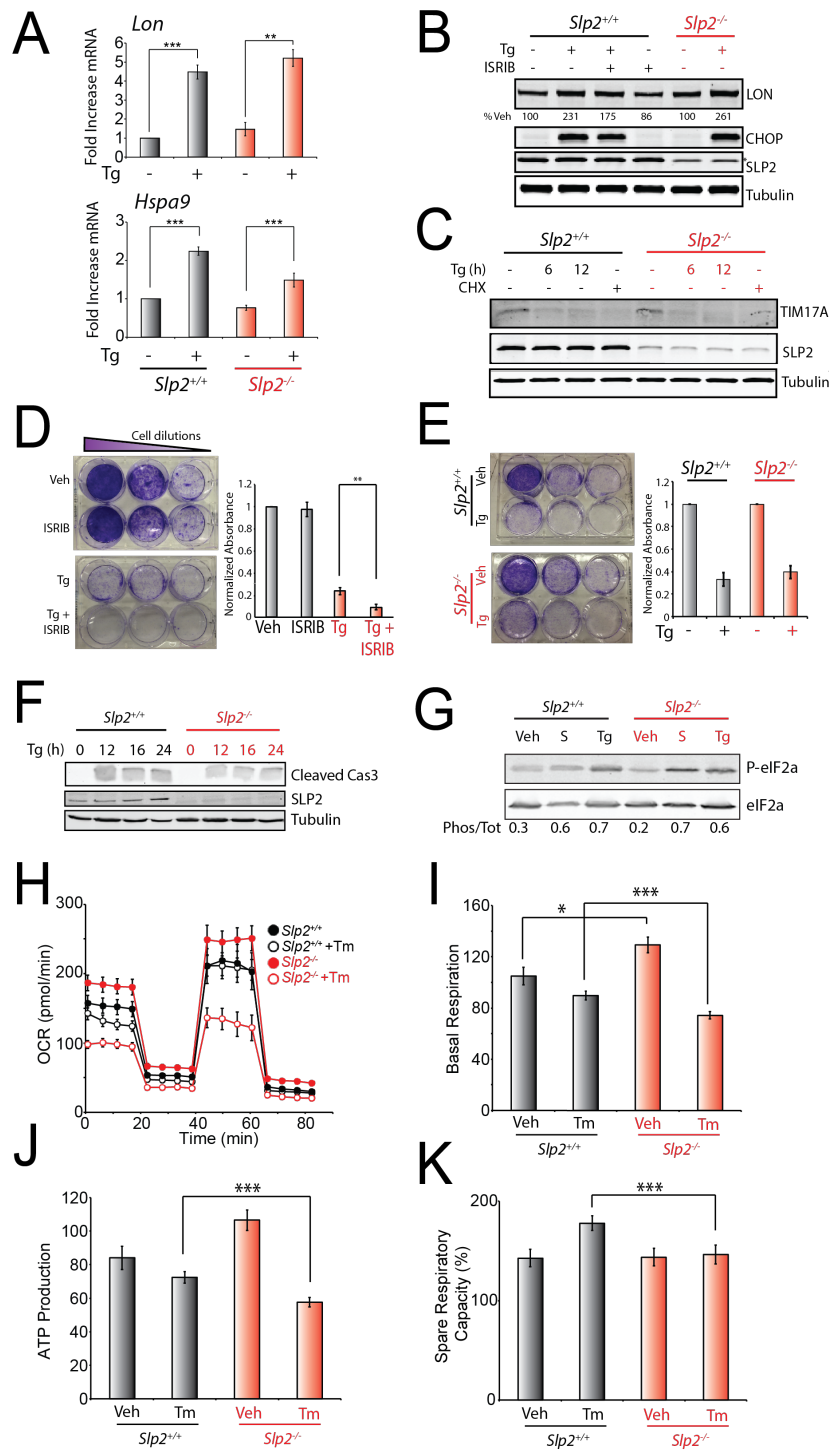


Figure S4 (Supplement to Figure 4)

- Graph showing *Lon* and *Hspa9* and *Chop* mRNA in *Slp2*^{+/+} and *Slp2*^{-/-} MEFs cells treated for 6 h with thapsigargin (Tg; 500 nM). Error bars SEM for n=3 independent experiments. **p < 0.01, ***p < 0.005 for a two-tailed paired t-test. The efficient Tg-dependent induction of these genes in *Slp2*^{-/-} MEFs confirms that PERK-regulated transcriptional signaling is not inhibited in these cells.
- Immunoblot of LON and CHOP in lysates prepared from *Slp2*^{+/+} and *Slp2*^{-/-} MEFs treated for 12 h with thapsigargin (Tg; 500 nM) and/or ISRIB (200 nM), as indicated. The relative expression of LON is quantified below the immunoblot. The efficient Tg-dependent increase in LON protein in *Slp2*^{-/-} MEFs confirms that PERK-regulated transcriptional signaling is not inhibited in these cells. Note we do observe a band in the SLP2 immunoblots in *Slp2*^{-/-} MEFs, which likely reflects a background band recognized by the SLP2 antibody.

- C.** Immunoblot of TIM17A in lysates prepared from *Slp2^{+/+}* and *Slp2^{-/-}* MEFs treated for 6 or 12 h with thapsigargin (Tg;500 nM) and/or cycloheximide (CHX;50 µg/mL), as indicated. The efficient Tim17A degradation observed in *Slp2^{-/-}* cells confirms that PERK-regulated translational signaling is not inhibited in these cells. Note we do observe a band in the SLP2 immunoblots in *Slp2^{-/-}* MEFs, which likely reflects a background band recognized by the SLP2 antibody.
- D.** Representative image from a colony formation assay performed in MEF^{WT} cells pretreated for 12 h with ISRIB (200 nM) and/or thapsigargin (Tg;500 nM). Following pretreatment, cells were plated at three different concentrations in a 6-well plate to allow single colony formation. Cells were then grown for 72 h prior to visualization using crystal violet staining. Graph showing the absorbance of solubilized crystal violet. Error bars show SEM from three independent experiments. ** p<0.01 for two tailed paired t-test.
- E.** Representative image from a colony formation assay performed in *Slp2^{+/+}* and *Slp2^{-/-}* MEFs pretreated for 12 h with thapsigargin (Tg;500 nM). Following pretreatment, cells were plated at three different concentrations in a 6-well plate to allow single colony formation. Cells were then grown for 72 h prior to visualization using crystal violet staining. The graph shows the quantified absorbance of solubilized crystal violet from wells. Error bars show SEM from three independent experiments.
- F.** Immunoblot of cleaved Caspase3 in lysates prepared from *Slp2^{+/+}* and *Slp2^{-/-}* MEFs treated for 12, 16 and 24 h with thapsigargin (Tg;500 nM).
- G.** Immunoblot of P-eIF2α and eIF2α in lysates prepared from *Slp2^{+/+}* and *Slp2^{-/-}* MEFs incubated for 2 h with Seahorse media at 37°C, CO2 free incubator or treated with thapsigargin (Tg;500 nM) for 2h at 37°C, 5% CO2. The ratio of P-eIF2α relative to total eIF2α is quantified below the immunoblot.
- H.** Representative plot from one experiment showing OCR in *Slp2^{+/+}* (black) or *Slp2^{-/-}* (red) MEFs pretreated for 6 h with tunicamycin (Tm; 1µg/ml) prior to analysis by Seahorse.
- I.** Graph showing basal respiration of *Slp2^{+/+}* and *Slp2^{-/-}* MEFs treated with tunicamycin (Tm; 1µg/ml) for 6 h before OCR measurements. Error bars show SEM for n=20 collected over two independent experiments. *p<0.05; ***p<0.005 for a two-tailed unpaired t-test.
- J.** Graph showing ATP production of *Slp2^{+/+}* and *Slp2^{-/-}* MEFs treated with tunicamycin (Tm; 1µg/ml) for 6 h before OCR measurements. Error bars show SEM for n=20 collected over two independent experiments. ***p<0.005 for a two-tailed unpaired t-test.
- K.** Graph showing Spare Respiratory Capacity of *Slp2^{+/+}* and *Slp2^{-/-}* MEFs treated with tunicamycin (Tm; 1µg/ml) for 6 h before OCR measurements. Error bars show SEM for n=20 collected over two independent experiments. *p<0.05 for a two-tailed unpaired t-test.